Pergamon

Int. J. Heat Mass Transfer. Vol. 40, No. 8, pp. 1907–1922, 1997

0017–9310/97 $17.00+0.00

PII: S0017-9310(96)00187-1

Flow visualization and numerical simulation of transverse and mixed vortex roll formation in mixed convection of air in a horizontal flat duct

M. Y. CHANG, C. H. YU and T. F. LIN†

Department of Mechanical Engineering, National Chiao Tung University, Hsinchu, Taiwan, Republic of China

(*Received* 19 *April* 1996 *and in final form* 24 *May* 1996)

Abstract—Combined experimental flow visualization and three-dimensional unsteady numerical simulation were carried out to investigate the formation of the traveling transverse and mixed vortex roll structures from the initially unidirectional, subcritical flow of air in a bottom heated horizontal flat duct when the Rayleigh number was raised to a supercritical level. In the study the Reynolds number was varied from 2.5 to 20 and the Rayleigh number from 1500 to 8000. Both the experiment and computation, being in qualitative agreement, indicated that in the early stage of the transient a pair of longitudinal rolls are induced in the side wall region; then new longitudinal rolls were induced near the existing ones. Meanwhile, weak transverse rolls were generated in the duct entry. As time proceeds, the transverse rolls grow in size and strength and slowly move downstream to push the longitudinal rolls in front of them out of the duct. At the same time new transverse rolls are generated in the duct entry. At a low Reynolds number ($Re \leqslant 5$) the transverse rolls are longer and stronger to expel all the longitudinal rolls out of the test section so that a pure and regular transverse vortex roll structure is formed. While at a higher Reynolds number ($Re \geqslant 7.5$) the transverse rolls are shorter and weaker and a few longitudinal rolls stay, all the time, near the duct sides, resulting in a mixed longitudinal and transverse roll structure. In the numerical simulation the temporal characteristics of the two vortex flow structures at the statistical state are also examined in detail.

1. INTRODUCTION

The buoyancy induced vortex flow structures in a mixed convective gas flow through a bottom heated horizontal flat duct play an important role in growing thin crystal film from chemical vapor deposition processes and recently they have been studied extensively [1]. Various vortex flow structures such as the steady and unsteady longitudinal rolls, traveling transverse rolls, mixed longitudinal and transverse rolls, and irregular cells have been reported in the literature. The formation of the longitudinal vortex flow is known to begin with the generation of a pair of longitudinal rolls near the duct sides and the subsequent generation of the longitudinal rolls near the existing ones. However, the detailed dynamic processes of how other vortex flows are formed from an initially simple unidirectional subcritical flow, when the governing parameters are raised to the supercritical levels, are still poorly understood. A well designed flow visualization experiment combined with the three-dimensional numerical simulation were carried out in the present study to unravel these dynamic processes for the formation of the moving transverse rolls and the mixed longitudinal and transverse rolls in an air flow through a bottom heated flat duct.

A comprehensive review of the literature on the longitudinal vortex rolls in a horizontal duct was already given in our previous study [2]. Here, only the literature relevant to the present study is briefly reviewed in the following.

In a mixed convective flow of fluid between two horizontal plates with the bottom plate at a higher uniform temperature than the top one, the critical Rayleigh number for the onset of secondary flow is at $Ra_c = 1708$. Beyond Ra_c steady longitudinal rolls prevail and the roll diameter is nearly equal to the duct height [3–6]. The vortex rolls become irregular for a high Gr/Re^2 [7, 8]. A flow regime map of the Reynolds number Re vs the Rayleigh number Ra was proposed for nitrogen gas to locate the boundaries among the flow with no roll, steady and unsteady rolls [9, 10]. The existence of the transverse thermoconvective rolls was proved with silicone oil as the working fluid [11], at a very low Reynolds number, $0.001 \leqslant Re \leqslant 0.01$. A refined flow regime map to include the transverse rolls was provided later [12, 13]. Recently, we reported a mixed roll pattern which is characterized by longitudinal rolls induced near the duct sides and transverse rolls in the duct core [14]. Also, the deformation of the transverse rolls was

† Author to whom correspondence should be addressed.

NOMENCLATURE

a, a'	dimensionless and dimensional time constants
A	aspect ratio, b/d
b	channel width
d	channel height
g	gravitational acceleration
Gr	Grashof number, $g\beta d^3(T_h - T_c)/\nu^2$
l, L	dimensional and dimensionless length of test section, l/d
Nu	local Nusselt number on the bottom plate
p	dimensionless dynamic pressure
Pr	Prandtl number
Ra	Rayleigh number, $g\beta d^3(T_h - T_c)/\nu\alpha$
Ra_c	critical Rayleigh number corresponding to the onset of convection in the form of longitudinal rolls
Re	Reynolds number, $\bar{W}d/\nu$
T, θ	dimensional and dimensionless temperature, $(T - T_c)/(T_{hf} - T_c)$
T_c	temperature of the cold surface
T_h	temperature of the hot surface
u, v, w	dimensionless velocity components scaled with $\bar{W}$
$\bar{W}$	average axial velocity
x, y, z	dimensionless Cartesian coordinates scaled with d.

Greek symbols

α	thermal diffusivity
β	thermal expansion coefficient
ν	kinematic viscosity.

Subscripts

f	final state
fd	fully developed state
i	initial state
max	maximum.

investigated. In all the literature reviewed above only the final flow structures at steady or statistical state were examined. The processes through which these structures are formed have not been explored and will be experimentally and numerically investigated in the present study. Attention will be focused on the subsequent evolution of the vortex flow after the change in the Reynolds or Rayleigh number by visualizing the flow from the top, end and side views. In the study the Reynolds number was varied from 2.5 to 20 and the Rayleigh number from 1500 to 8000.

2. EXPERIMENTAL APPARATUS AND PROCEDURES

2.1. *Experimental apparatus*

A sketch of the established test apparatus for the mixed convection of air in a bottom heated horizontal plane channel and the adopted coordinate system are shown in Fig. 1. The test section is a rectangular duct 240 mm wide and 300 mm long with a gap width of 20 mm between the hot and cold walls; thus the aspect ratio of the duct is 12. The lower plate of the test section is made of a 15 mm thick, high purity copper plate and is electrically heated by d.c. power supplies. The heaters glued onto the outside surface of the bottom wall were divided into 10 segments in the flow direction and each heater was controlled independently by a GW GPC 3030D laboratory power supply. The high thermal conductivity, density and large thickness of the copper plate can minimize the nonuniformity and unsteadiness in the bottom wall temperature. The width of the lower plate is 40 mm larger than that of the test section in order to reduce the edge effect in the spanwise direction of the test section. The upper plate is cooled by distilled water flowing above it. The distilled water is maintained at constant temperature by a heat exchanger. The heat exchanger can control the temperature of the distilled water within ± 0.1°C. The volume flowrate of the distilled cooling water is adjusted carefully so that the temperature difference in the cooling water over the glass plate is within ± 0.1°C. The water head is also suitably adjusted to minimize any possible deformation of the glass plate. The side walls of the test section are made of 5 mm thick plexiglass.

The temperature of the lower plate is measured by 13 calibrated and electrically insulated T-type thermocouples embedded in the plate. The temperature of the upper plate is measured by 6 T-type thermocouples stuck to the inside surface of the plate. The temperature of both plates can be maintained nearly uniform and at constant values with deviations ranging from ± 0.05°C to ± 0.12°C, depending on the Rayleigh number tested. For each experiment the top plate temperature is kept at the same value as that of the inlet air flow for the purpose of eliminating the formation of a thermal boundary layer on the top wall.

The open loop mixed convection apparatus begins with the air regulated from a 600 psi and 50 000 ft^3 high pressure air tank which is passed through a settling chamber, a contraction nozzle and a developing channel before entering the test section. In the settling chamber turbulence is suppressed by firstly passing the air through two fine mesh screens, then a honeycomb section and finally four fine mesh screens. The nozzle with a contraction ratio of 20 : 1 has been designed to eliminate flow separation, minimize turbulence and

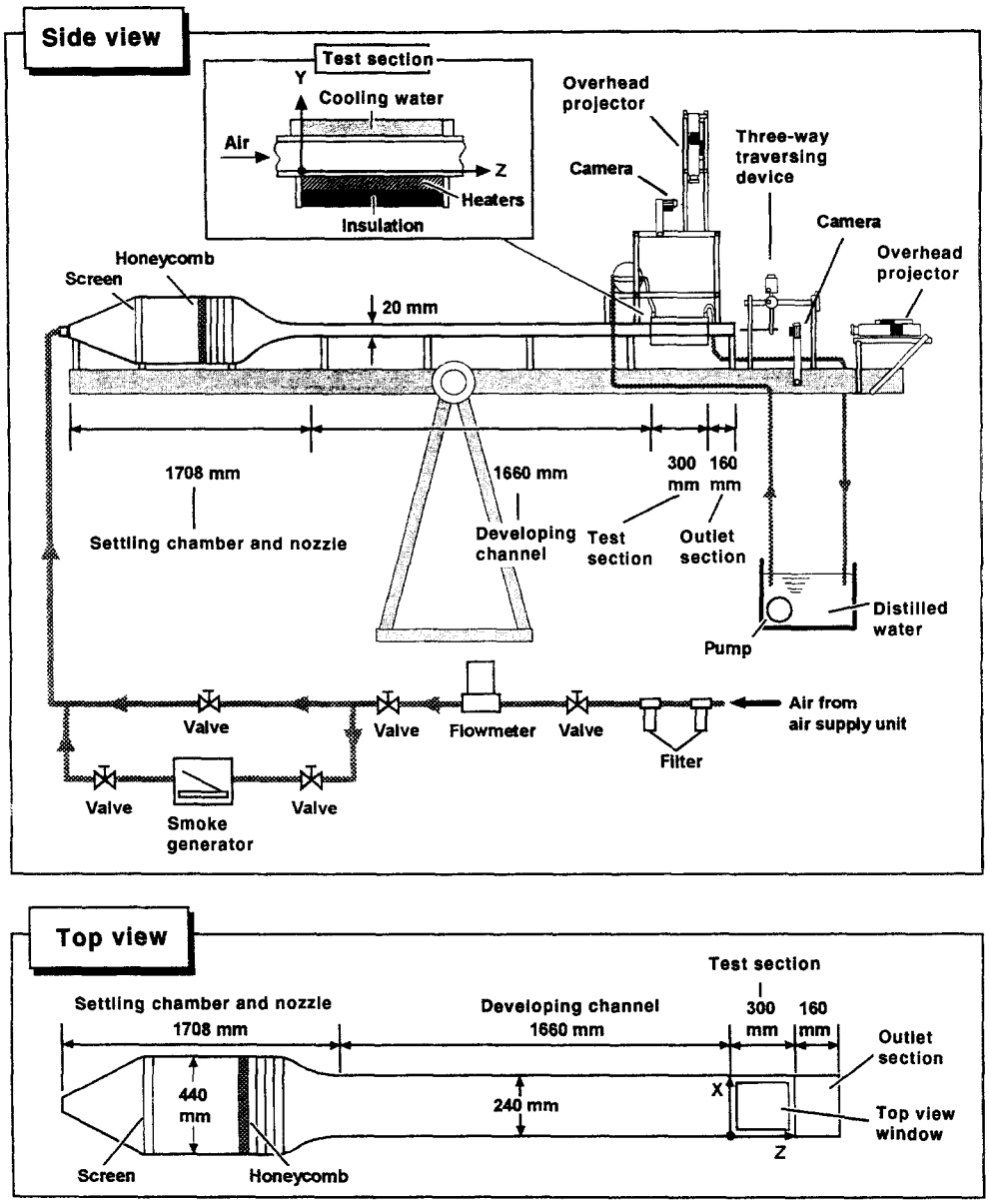

Fig. 1. Schematic of test apparatus and the chosen coordinate system.

provide a nearly uniform velocity at the inlet of the developing section. The developing section is 1600 mm in length, approximately 83 times the channel height. This ensures the flow is fully developed at the inlet of the test section for $Re \leqslant 50.0$. A 160 mm outlet section is added to the exit end of the test section to reduce the disturbance resulting from discharging the flow into the ambient. The settling chamber and the contraction nozzle are made of stainless steel, whereas the developing channel and the outlet section are made of 5 mm thick plexiglass. The whole test apparatus is placed in a quiescent house to eliminate any possible disturbance from the ambient surrounding the house. The entire loop including the settling chamber, contraction nozzle, developing channel, test section and outlet section is thermally insulated with the superlon insulator 20 mm thick and is mounted on a rigid supporting frame.

The volume flow rate of air is controlled and measured by a Hasting HFC flow controller with an accuracy better than 1%. The flow measuring system is calibrated periodically by a Brooks bell prover with an accuracy of 0.2%. The operating condition of the flow meter in actual measurement is adjusted to a condition similar to that of a calibration stand. The mean air speed in the test section is calculated from the total flow rate.

To measure the velocity and temperature of the air flow in the test section, probes are inserted from the downstream end of the test section. The probes are supported by a three-way traversing device. Velocity is measured by a hot-wire probe. For calibrating the

hot-wire, the pipe flow method in which the probe is placed in the center of a fully developed laminar pipe flow is used. The total flow rate is measured and the pipe center velocity is calculated from the parabolic distribution. The temperature is measured by a thermocouple probe which is an OMEGA (model HYP-O) extremely small T-type thermocouple (33 gauge) implanted in a 1 in long stainless steel hypodermic needle.

2.2. *Data uncertainty*

The data acquisition and control system and various instruments including: a PC 486-66, multiplexers (Computer Product RTP 743 series), a digital barometer (Setra System 361B), reference junctions (Celsco Transducer Products BRJ 14), laboratory power supplies (GW GPC 3030D), OMEGA type T thermocouples, a Hasting HFC flow controller and a reduction software, were calibrated and adjusted end-to-end on site by Instrument Calibration Section, Q.A. Center, Chung Shan Institute of Science and Technology (CSIST), Taiwan with the transfer standards that the calibration hierarchy can trace back to the standards of National Institute of Standard and Technology (NIST), U.S.A. Before performing the end-to-end calibration all the sensors and transducers used were transported to CSIST for calibration or adjustment with the inter-lab standards based on the test point that was encountered in the present test in order to get the best calibration curve-fit data. The main purpose of this calibration is to reduce any possible bias between the true physical values and the readouts of the sensors or transducers. The data reduction error is reduced further by using the best nonlinear least square calibration curve-fits and by selecting a suitable gain code of the multiplexers. The system is well grounded and the electric noises are suitably filtered out. Fixed physical or simulated signals are then applied in the data uncertainty test. Samples higher than 32 are measured at each test point during the data uncertainty test. Uncertainties in the Rayleigh number, Reynolds number and other independent parameters were calculated according to the standard procedures established by Kline and McClintock [15] and Abernethy and Thompson [16]. Uncertainties due to the control unsteadiness and temperature nonuniformity are also accounted for in the data uncertainty evaluation. In addition, uncertainties of the thermophysical properties of the air were also included in the analysis. The detailed uncertainty analysis indicated that uncertainties of temperature, volume flow rate, dimensions, Reynolds number and Rayleigh number measurements are estimated to be less than $\pm 0.15^{\circ}C$, $\pm 5\%$, ± 0.05 mm, $\pm 6\%$ and $\pm 6\%$, respectively, in this low Reynolds and Rayleigh number experiment.

2.3. *Preliminary investigation of flow field*

Firstly, the main forced flow is investigated to check its fully developed condition at the entrance of the test section with no heat input to the bottom plate. The results indicate that at the test section inlet the velocity profile is fully developed and is in good agreement with the analytical results given by Shah and London [17]. Additionally, the turbulence intensity is found to be less than 0.7%.

Flow visualization is conducted to observe the secondary flow patterns by injecting smoke at some distance ahead of the settling chamber. It is carried out by using a 1.5–2.5 mm plane light beam to shine through the flow field containing tiny incense particles as the light scattering centers and a sharp contrast could be achieved between the duct walls and the smoke.

In all the experiments reported below, we first imposed a fully developed flow in the entire test section and then turned on the power supply to the bottom plate and in the mean time circulated chilled water over the top plate. The Rayleigh number *Ra* is raised to 1500 and stabilized for half an hour. After this we started the transient processes and visualized the evolution of the vortex flow.

3. NUMERICAL SIMULATION

3.1. *Mathematical modeling*

Considered in the numerical simulation is a mixed convective air flow with a mean velocity $\bar{W}$ in a differentially heated horizontal rectangular duct, as schematically shown in Fig. 2 along with the chosen coordinates. The flow enters the duct at a uniform temperature T_c and the top plate of the duct is also kept at this uniform temperature during the entire transient. Initially the bottom plate temperature is kept at a uniform subcritical level T_{hi} so that the Rayleigh number associated with the corresponding temperature difference $(T_{hi}-T_c)$ is below 1708. After a sufficiently long period of time a steady subcritical flow prevails in the duct. Then at a certain instant

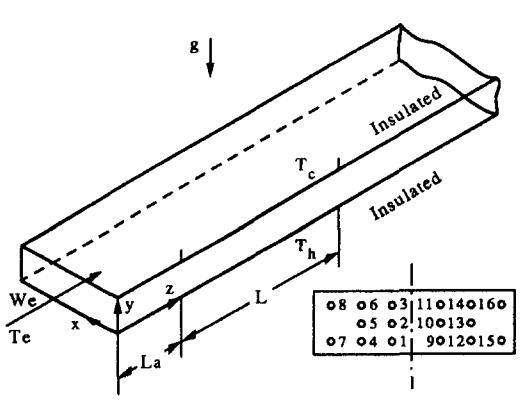

Fig. 2. Schematic of the physical system and the detection points at a cross section. (The x and y coordinates at various points are as follows: 1 (6.79, 0.17), 2 (6.79, 0.5), 3 (6.79, 0.83), 4 (9.16, 0.17), 5 (9.16, 0.5), 6 (9.16, 0.83), 7 (11.41, 0.17), 8 (11.41, 0.83), 9 (5.21, 0.17), 10 (5.21, 0.5), 11 (5.21, 0.83), 12 (2.84, 0.17), 13 (2.84, 0.5), 14 (2.84, 0.83), 15 (0.59, 0.17), 16 (0.59, 0.83).)

of time designated as $t = 0$, the bottom plate temperature is raised to a uniform supercritical level T_{hf}. In view of the large thermal inertia of the bottom plate in the experimental setup, the rise in the bottom plate temperature with time is described as $T_h = T_{hi} + (T_{hf} - T_{hi})(1 - e^{-a't})$, where a' is the time constant of the temperature rise and will be selected to comply with the experiment. Note that since the thermal conductivity of the plexiglass side walls is ($k_s = 0.21$ W m^{-1}°C^{-1}) much higher than that of air ($k_{air} = 0.026$ W m^{-1}°C^{-1}), perfect thermal conduction is assumed in the side walls. It should be noted that upstream and downstream of the heated section of the duct is thermally well insulated. When the length, time and velocity and temperature are respectively scaled with the duct height d, mean convection time $d/\bar{W}$, mean velocity $\bar{W}$ and temperature difference $\Delta T (= T_{hf} - T_c)$, the basic non dimensional equations describing the formation of the buoyancy driven vortex flow of a Boussinesq fluid from the initially unidirectional subcritical flow studied here are:

$$\frac{\partial u}{\partial x} + \frac{\partial v}{\partial y} + \frac{\partial w}{\partial z} = 0 \tag{1}$$

$$\frac{\partial u}{\partial \tau} + u\frac{\partial u}{\partial x} + v\frac{\partial u}{\partial y} + w\frac{\partial u}{\partial z} = -\frac{\partial p}{\partial x} + \frac{1}{Re}\left(\frac{\partial^2 u}{\partial x^2} + \frac{\partial^2 u}{\partial y^2} + \frac{\partial^2 u}{\partial z^2}\right) \tag{2}$$

$$\frac{\partial v}{\partial \tau} + u\frac{\partial v}{\partial x} + v\frac{\partial v}{\partial y} + w\frac{\partial v}{\partial z} = -\frac{\partial p}{\partial y} + \frac{1}{Re}\left(\frac{\partial^2 v}{\partial x^2} + \frac{\partial^2 v}{\partial y^2} + \frac{\partial^2 v}{\partial z^2}\right) + \frac{Gr}{Re^2}\theta \tag{3}$$

$$\frac{\partial w}{\partial \tau} + u\frac{\partial w}{\partial x} + v\frac{\partial w}{\partial y} + w\frac{\partial w}{\partial z} = -\frac{\partial p}{\partial z} + \frac{1}{Re}\left(\frac{\partial^2 w}{\partial x^2} + \frac{\partial^2 w}{\partial y^2} + \frac{\partial^2 w}{\partial z^2}\right) \tag{4}$$

$$\frac{\partial \theta}{\partial \tau} + u\frac{\partial \theta}{\partial x} + v\frac{\partial \theta}{\partial y} + w\frac{\partial \theta}{\partial z} = \frac{1}{Re - Pr}\left(\frac{\partial^2 \theta}{\partial x^2} + \frac{\partial^2 \theta}{\partial y^2} + \frac{\partial^2 \theta}{\partial z^2}\right) \tag{5}$$

subject to the following initial and boundary conditions:

$\tau = 0,$

(u, v, w, θ) = steady subcritical flow and temperature fields calculated from computation [2] $\tau > 0$

$x = 0, A$

$$u = v = w = 0$$
$$\theta = (1-y)\left[\frac{Ra_i}{Ra_f} + \left(1 - \frac{Ra_i}{Ra_f}\right)(1 - e^{-a\tau})\right]$$

$y = 0, L_a \leqslant z \leqslant L + L_a \qquad u = v = w = 0$

$$\theta = \frac{Ra_i}{Ra_f} + 1\left(\frac{Ra_i}{Ra_f}\right)(1 - e^{-a\tau})$$

$y = 0, 0 \leqslant z < L_a, z > L + L_a$

$$u = v = w = 0 \quad \frac{\partial \theta}{\partial y} = 0$$

$y = 1, L_a \leqslant z \leqslant L + L_a \qquad u = v = w = 0 \quad \theta = 0$

$y = 1, 0 \leqslant z < L_a, z > L + L_a$

$$u = v = w = 0 \quad \frac{\partial \theta}{\partial y} = 0$$

$z = 0 \qquad u = v = 0 \quad w = w_{fd}, \theta = 0$

$z \to \infty \qquad \frac{\partial u}{\partial z} = \frac{\partial v}{\partial z} = \frac{\partial w}{\partial z} = \frac{\partial \theta}{\partial z} = 0 \tag{6}$

where the inlet velocity w_{fd} in the far upstream $z \to -\infty$ is assumed as fully developed

$$w_{fd} = \left(\frac{m+1}{m}\right)\left(\frac{n+1}{n}\right) \times [1 - (|2y-1|)^n]\left[1 - \left(\left|\frac{2x}{A} - 1\right|\right)^m\right] \tag{7}$$

with the values of the constants m and n depending on the aspect ratio A [17].

The nondimensional groups which appeared in the above formation are defined as

$$Re = \frac{\bar{W}d}{\nu} \quad Pr = \frac{\nu}{\alpha}$$

$$Gr = \frac{g\beta(T_h - T_c)d^3}{\nu^2} \quad A = \frac{b}{d} \quad a = a'\frac{\bar{W}}{d}. \tag{8}$$

To account for the upstream diffusion at low Reynolds number flow, an upstream insulated section of length L_a was added to the heated section as shown in Fig. 2. The selection of the proper L_a will be discussed in the next section. The local Nusselt number which signifies the heat transfer from the bottom heated plate to the channel flow is defined and evaluated as

$$Nu \equiv \frac{hd}{k} = \frac{q''_w}{(T_{hf} - T_c)}\frac{d}{k} = -\left.\frac{\partial \theta}{\partial y}\right|_{y=0} \tag{9}$$

where q''_w is the local convective heat flux and k is the thermal conductivity of the fluid in the duct.

3.2. *Solution method*

In view of the nonlinearity in the inertia terms, the basic flow equations were solved numerically. In particular, the projection method [18] was chosen to integrate the equations on a staggered grid system. This splitting (fractional step) method consists of two steps. First, a provisional velocity field was explicitly computed, ignoring the pressure gradient. Then, it was corrected by including the pressure effect and by enforcing the mass conservation. The pressure dis-

tribution is obtained from solving the pressure Poisson equation by the vectorized SOR method.

To enhance numerical accuracy and stability, all the spatial derivatives were discretized by the fourth-order central differences [19], except the convective terms which were treated by the third-order upwind difference proposed by Kawamura *et al.* [20]. For the nodes near the boundaries, the usual second order central difference was employed to facilitate the treatment of the boundary condition. This is not expected to significantly affect the accuracy of the solution since the flow either is rather slow due to the no-slip condition near the solid boundaries or changes slowly near the free boundaries. To allow for the possible presence of asymmetric flow with respect to the central vertical plane at $x = A/2$ for the time dependent flow induced at high Gr/Re^2, the computation domain includes both the left-half and right-half of the channel. Although the downstream boundary conditions were exactly specified at $z \to \infty$, only a finite unheated section is added in the downstream to facilitate the numerical analysis. Both this unheated section and the upstream insulated section must be long enough so that the solution for the problem is independent of their sizes. Numerical tests indicated that the suitable length for the upstream and downstream unheated section is $0.2L$ and $0.47L$, respectively.

Time advancement may be done either implicitly or explicitly. The first-order Euler explicit scheme was employed here since it has a much lower computational cost per time step and requires much less computer memory allocation than any equivalent implicit implementation. We also found that the first-order scheme was sufficiently accurate to resolve the smallest physical time scale. The stability of the scheme is limited by the requirement that the Courant number must be less than unity [21]. To insure the numerical convergence, the Courant number is set below 0.05 in the computation, which leads to

$$\Delta t < 0.05 \times \text{minimum}\left(\frac{\Delta x}{u_{\max}}, \frac{\Delta y}{v_{\max}}, \frac{\Delta z}{w_{\max}}\right). \quad (10)$$

The sequence of numerical operation is as follows:

(1) Explicitly calculate the provisional velocity.

(2) Solve the pressure equation by the vectorized Gauss-Seidel method with successive over-relaxation. The solution for the pressure is considered as convergent when the mean relative pressure difference between two consecutive iterations is below 10^{-4}, i.e.

$$\sum_{i,j,k} \frac{|(p_{i,j,k}^{n+1})^{m+1} - (p_{i,j,k}^{n+1})^{m}|}{|(p_{i,j,k}^{n+1})^{m+1}|} / (I \times J \times K) < 10^{-4} \quad (11)$$

where i, j, k are the indices of the nodes in the x, y, z directions, respectively, m is the iteration number and I, J, K are the total numbers of nodes in the x, y, z directions, respectively. This ensures the mass imbalance at each node is less than 10^{-4} of the inlet mass flow rate.

(3) Explicitly calculate the desired velocity and temperature fields at the new time step.

Procedures (1)–(3) were repeatedly applied from the initiation of the transient to a final steady state or to a statistical state when the flow was no longer steady for a long time.

Stringent program tests were carried out in the previous study [2] to verify the proposed solution method. Very good agreement between the present predictions and published results in the literature was shown by comparing our predictions with the experimental data for the mixed convective vortex flow in a horizontal flat duct [7, 10]. The comparison of our predicted velocity profile for a typical case with $Pr = 7$, $Ra = 2420$ and $A = 3.63$ with the experimental data of Ouazzani *et al.* [13] also shows good agreement. Finally, a grid-independence test was performed. Sampled results from this test indicate that the oscillation frequency of the flow, a very important characteristic of the oscillatory flow, calculated from the $91 \times 15 \times 121$, $101 \times 15 \times 121$, $91 \times 25 \times 121$ and $91 \times 15 \times 131$ grids for a typical case with $Pr = 0.71$, $Re = 10$, $Ra = 5000$, $A = 12$ and $L = 15$ is 0.513, 0.513, 0.509 and 0.536, respectively. The differences between them all are less than 4%. Moreover, the predicted time oscillations of the axial velocity w and temperature θ at a large time computed from the four different grid densities also show good agreement. Comparison of the present numerical simulation with our experimental results will be discussed later. Through these program tests, the adopted solution procedures are considered to be suitable for the present study.

4. RESULTS AND DISCUSSION

In the following, selected results from the present study will be presented to illustrate the formation of the transverse and mixed vortex roll structures from the initially unidirectional flow and the associated flow and thermal characteristics.

4.1. *Experimentally observed formation of vortex structures*

The formation of the transverse and mixed roll structures from the initially forced convective unidirectional flow observed in this experiment will be investigated first. Before presenting the results it should be noted that the top view flow photos can illustrate the vortex flow formation most clearly and will be examined carefully in the following. To unravel the formation of the moving transverse rolls, the initially unidirectional flow is obtained at first by setting the Rayleigh number at a subcritical value for a long period of time at a fixed Reynolds number and then raising the Rayleigh number to a desired supercritical level at which the transverse rolls are expected to appear. Due to the large thermal inertia of the bottom (copper) plate, it takes about one to two minutes to raise Ra to the required level. The evolution

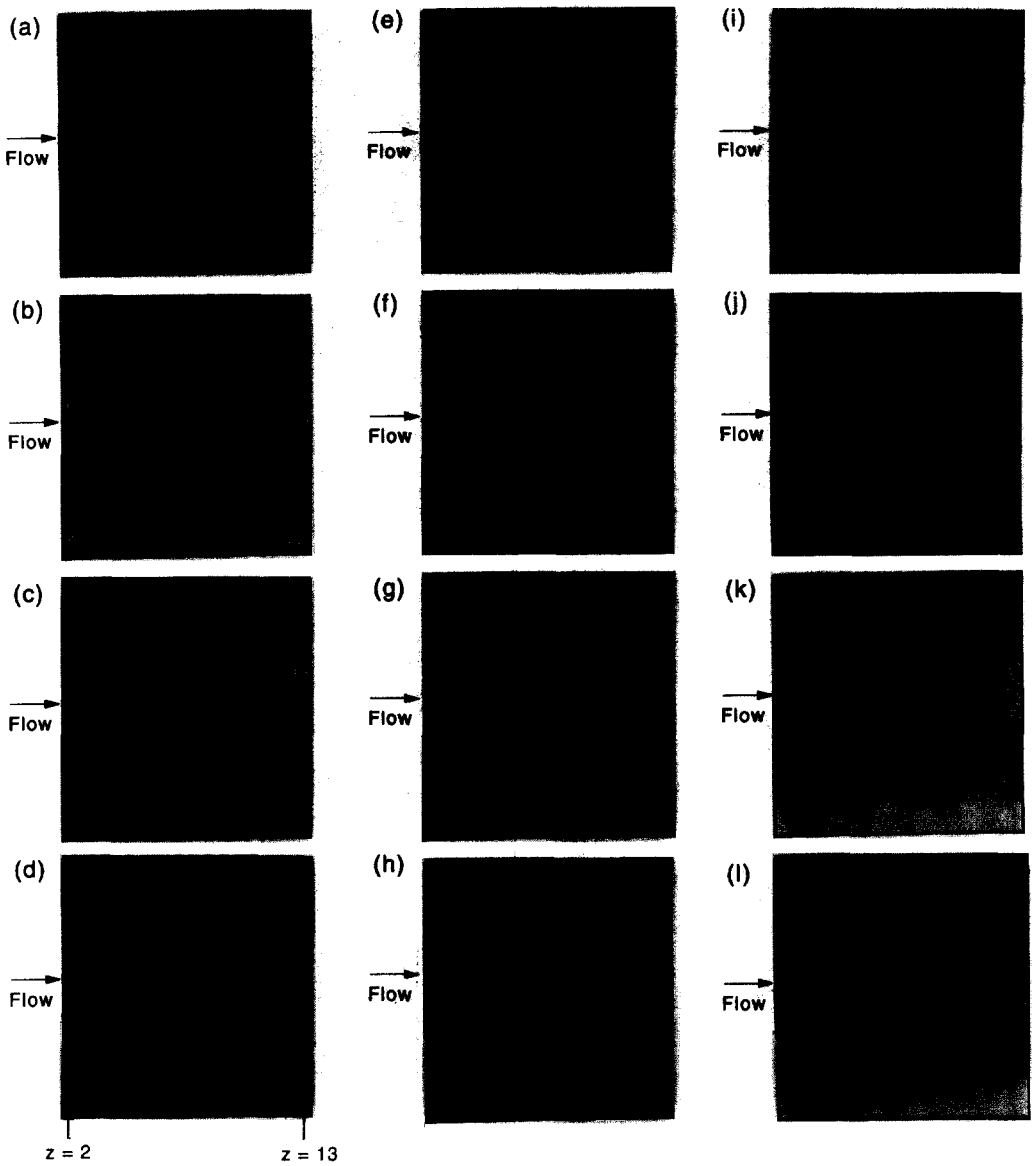

Fig. 3. Flow pattern transformation from the unidirectional flow to the transverse rolls by raising Ra from 1500 to 4300 in 110 s at $Ra = 5$ and $t =$ (a) 0 s (b) 33 s (c) 51 s (d) 60 s (e) 64 s (f) 87 s (g) 95 s (h) 101 s (i) 120 s (j) 154 s (k) 530 s and (l) 600 s ($t_p = 7.4$ s).

of the transverse vortex flow patterns in this simple experiment for a typical case in which Ra is raised from 1500 to 4300 in 110 seconds with $Re \approx 5$ is portrayed in Fig. 3. The instant at which we start raising the Rayleigh number to 4300 is designated as time $t = 0$ s. The results indicate that shortly after the start of the transient at $t = 33$ s two strong longitudinal vortex rolls already appear near each side wall of the duct along with a number of weak rolls in the duct core (Fig. 3(b)). As time proceeds, the existing rolls are strengthened and new longitudinal rolls are gradually induced; meanwhile extremely weak transverse rolls are generated in the entry region of the duct, as is evident from a snapshot of the flow from the top view, shown in Fig. 3(c). Then the transverse rolls grow in size and strength and are pushed by the mean flow to move slowly downstream. In the meantime new transverse rolls are generated in the duct entry. As the transverse rolls travel downstream, they push the longitudinal rolls in front of them forward, but they are also blocked to a certain degree by these longitudinal rolls (Fig. 3(d)–(h)). This mutual interaction of the rolls causes the transverse rolls to become distorted and curved toward the duct inlet and the longitudinal rolls also become curved. The resulting flow patterns at these intermediate time steps are rather complicated. Later when the highly distorted longitudinal rolls are pushed out of the duct, the transverse rolls gradually straighten up (Fig. 3(i)–(j)). With a further elapse of time the longitudinal rolls near the duct sides gradually disappear (Fig. 3(k)). Finally the pure and regular transverse rolls occupy the entire

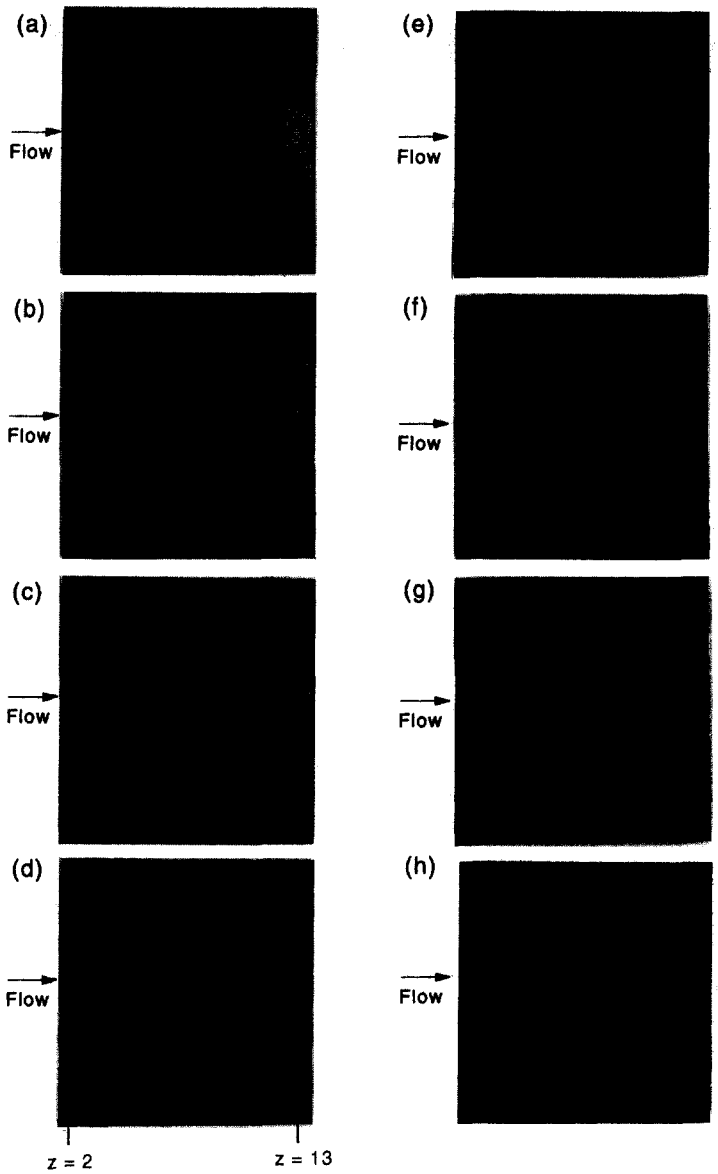

Fig. 4. Flow pattern transformation from the unidirectional flow to the mixed longitudinal and transverse rolls by raising *Ra* from 1500 to 4200 in 90 s at *Re* = 10 and *t* = (a) 0 s (b) 35 s (c) 49 s (d) 56 s (e) 69 s (f) 86 s (g) 220 s and (h) 300 s (t_p = 3.8 s).

duct (Fig. 3(l)). The flow is found to be time periodic with the period $t_p = 7.4$ s.

An exemplified case is shown in Fig. 4 to show the formation of the mixed roll structure. The results indicate that upon raising the Rayleigh number to 4200 at $t = 0$, weak longitudinal rolls are subsequently induced near the duct sides in the initially subcritical flow with $Re = 10$ and $Ra = 1500$. At this higher Reynolds number the longitudinal rolls do not fill the entire duct so that the flow in the duct core is still forced convective and unidirectional (Fig. 4(c)). Later at $t = 56$ s two short and relatively weak transverse rolls appear in the downstream core region (Fig. 4(d)). As time advances, the transverse rolls gradually move downstream and expand in the spanwise direction and their vortex intensity increases slowly (Fig. 4(e)–(g)). Meanwhile, new transverse rolls are induced in the entry region. In addition, the longitudinal rolls also get stronger. Note that the growth of the transverse rolls with time and the growth of the longitudinal rolls with the axial distance cause the longitudinal rolls to be squeezed to a certain degree and the transverse rolls to become slightly bent and distorted. In the interboundary region between the longitudinal and transverse rolls the flow is unstable and irregular. Eventually, a mixed roll structure is formed (Fig. 4(h)). The flow is also noted to be time periodic with $t_p = 3.8$ s.

4.2. *Numerically predicted formation of vortex structures*

The numerical predicted vortex flow formation of the moving transverse rolls to simulate the above experiment can be conveniently illustrated by the results for the local Nusselt number distributions on the bottom plate and the air temperature in the middle horizontal plane at $y = 1/2$. Fig. 5(a)–(h) presents these results to show the flow formation from an initially steady subcritical flow at $Re = 5$ and $Ra = 1500$ to a final traversing transverse vortex flow at $Re = 5$ and $Ra = 4300$. To model the thermal inertia of the bottom plate in the experiment, the time constant a is set at 0.35 in this numerical computation. The results in Fig. 5 clearly indicate that immediately after the start of the transient at $t = 15.3$ s near each side wall a weak longitudinal vortex roll is induced in the initially unidirectional flow. Meanwhile, a pair of weak transverse rolls are induced in the duct entry. Later as the buoyancy gets stronger with time, the rolls grow in size and strength and more longitudinal rolls are induced (Fig. 5(c)). In the entry half of the duct core, a number of recirculating cells prevail. As the process proceeds, at $t = 45.9$ s the cells merge together to form short distorted transverse rolls which slowly move downstream. Additionally, a new pair of transverse rolls are generated in the duct entry. The transverse rolls are found to merge with the longitudinal rolls to form curved rolls (Fig. 5(d)). With a further increase in time the transverse portion of the curved rolls during movement downstream expand in the spanwise direction to become longer. This causes the longitudinal rolls near the duct sides to gradually shrink and finally disappear. At this time the newly generated transverse rolls in the duct inlet extend nearly to the side walls. When the transverse rolls slowly move downstream, the curved rolls are pushed out of the duct (Fig. 5(e)–(g)). Finally, a regular transverse vortex flow is reached at $t = 137.7$ s and the flow gradually evolves to a time periodic state. A close inspection of the computed time records of the air temperature in the time periodic flow at selected detection points specified in Fig. 2 at selected cross-sections suggests that the entire flow oscillates at a single frequency ($F = 0.56$ or $f = 2.88$ Hz) and the oscillation amplitude increases significantly with the axial distance in the duct entry $z < 5$, where the transverse rolls are generated and are developing as they move downstream. As the transverse rolls become fully developed at $z \geqslant 5$ the oscillation amplitude does not vary with the axial distance but changes substantially with the vertical coordinate. A small sample of the time records for θ and w is shown in Fig. 6. It is also noted that the flow in the entire transient including the initial development and final periodic state is symmetric with respect to the center vertical plane at $x = 6$. It is important to realize that the numerically predicted transverse vortex flow evolution discussed above is in qualitative agreement with that observed in the experiment shown in Fig. 3.

In simulating the formation of the mixed roll structure, the initially unidirectional flow at $Re = 10$ and $Ra = 1500$ is first numerically obtained. Then the Rayleigh number is raised to 4200 at $t = 0$ with the time constant a chosen to be 0.2 to account for the thermal inertia of the bottom plate. The subsequent flow development is again illustrated by the distributions of the local Nusselt number and air temperature at the middle horizontal plane and is shown in Fig. 7(a)–(h). The results clearly demonstrate that as the transient starts the longitudinal rolls are successively induced, first near the side wall regions and then extending toward the duct core. At $\tau = 15$ ($t = 38.3$ s) the entire duct is filled with the longitudinal rolls. Later, as the buoyancy strengthens, a pair of weak and short transverse rolls are generated in the core region near the duct inlet. With a further increase in time the transverse rolls move downstream and get stronger and larger. The longitudinal rolls ahead of the transverse rolls are gradually pushed out of the duct and the longitudinal rolls adjacent to the transverse rolls merge with the transverse rolls (Fig. 7(e)). Meanwhile, new and longer transverse rolls are induced in the duct entry. As time proceeds, the flow slowly evolves to a time periodic state ($\tau_p = 1.88, t_p = 4.8$ s) as $\tau > 60$. The prevalent periodic flow is characterized by two longitudinal rolls near each side wall and traversing transverse rolls in the duct core (Fig. 7(g)–(h)). Like the experimental observation, in the interboundary region between the longitudinal and transverse rolls the numerically predicted flow is somewhat irregular. Also, it should be noted that due to the growth of the longitudinal rolls with the axial distance, the transverse rolls are squeezed to a certain degree and become shorter as they travel downstream. Checking the computed time histories of θ and w shown in Fig. 8(a)–(b) reveals that in the transverse roll region the flow oscillation is much stronger than that in the longitudinal roll region. Additionally, in the transverse roll region the oscillation amplitude is significantly dependent on the vertical position but changes slightly with the axial distance. However, in the longitudinal roll region an increase in the oscillation amplitude with distance from the side wall is observed (Fig. 8(b)).

A comparison of the above numerically predicted evolution of the mixed roll structure with that visualized in the experiment shown in Fig. 4 indicates that qualitative agreement is again reached. However, in the numerical prediction the longitudinal rolls were found to fill the entire duct during the transient stage of flow development. This is not observed in the experiment in which the duct is only partially occupied by the longitudinal rolls.

5. CONCLUDING REMARKS

Through a combined experimental flow visualization and three-dimensional unsteady numerical simulation, the present study demonstrates the

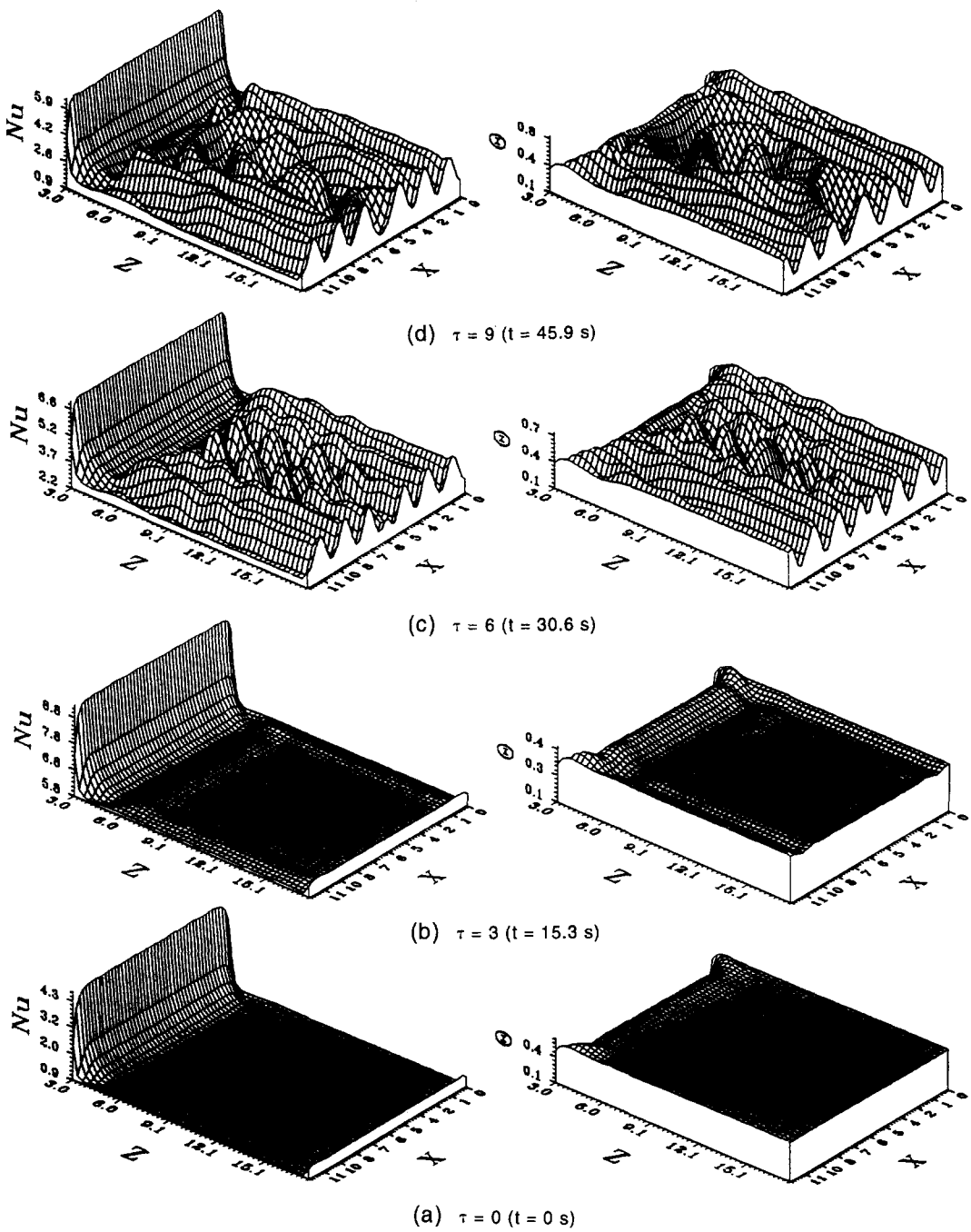

Fig. 5. The local Nusselt number distribution on the bottom plate and the temperature distribution in the middle horizontal plane ($y = 0.5$) for $Re = 5$ and $Ra = 4300$ at eight selected time instants (a) $\tau = 0$ ($t = 0$); (b) $\tau = 3$ ($t = 15.3$ s); (c) $\tau = 6$ ($t = 30.6$ s); (d) $\tau = 9$ ($t = 45.9$ s); (e) $\tau = 15$ ($t = 76.5$ s); (f) $\tau = 18$ ($t = 91.8$ s); (g) $\tau = 21$ ($t = 107.1$ s); (h) $\tau = 27$ ($t = 137.7$ s). (*Continued opposite.*)

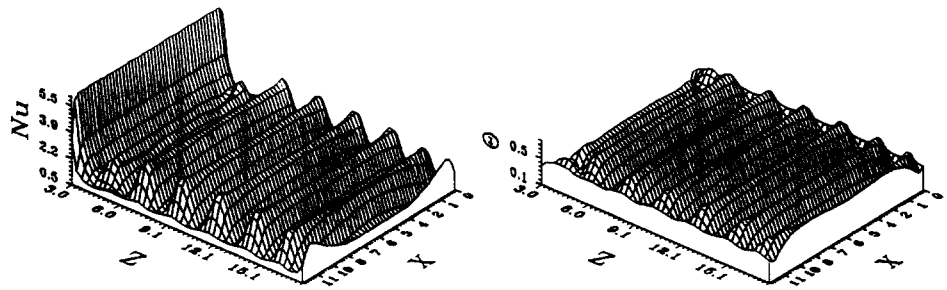

(h) τ = 27 (t = 137.7 s)

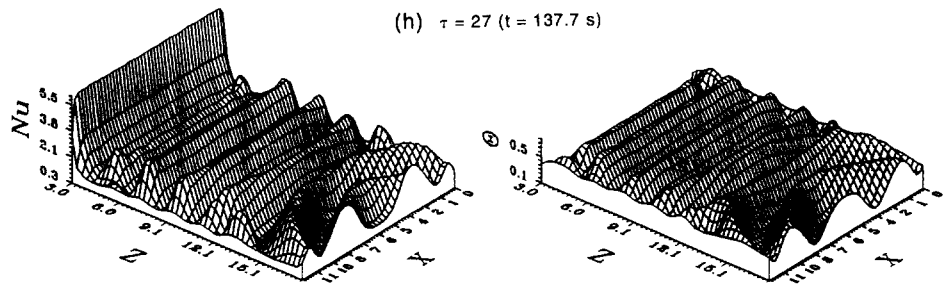

(g) τ = 21 (t = 107.1 s)

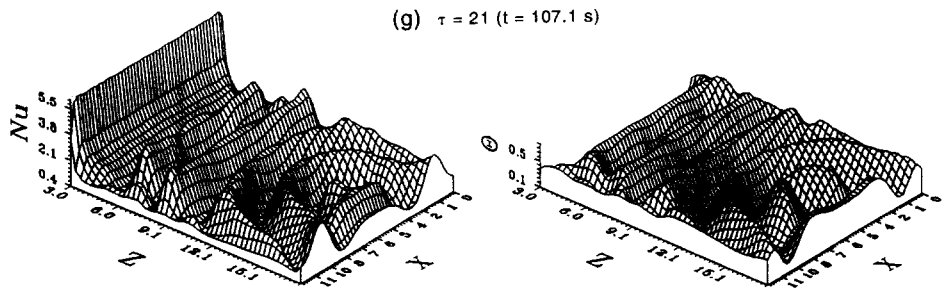

(f) τ = 18 (t = 91.8 s)

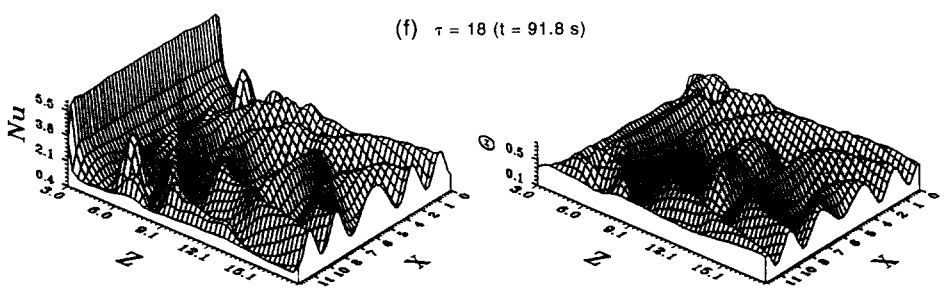

(e) τ = 15 (t = 76.5 s)

Fig. 5—*continued.*

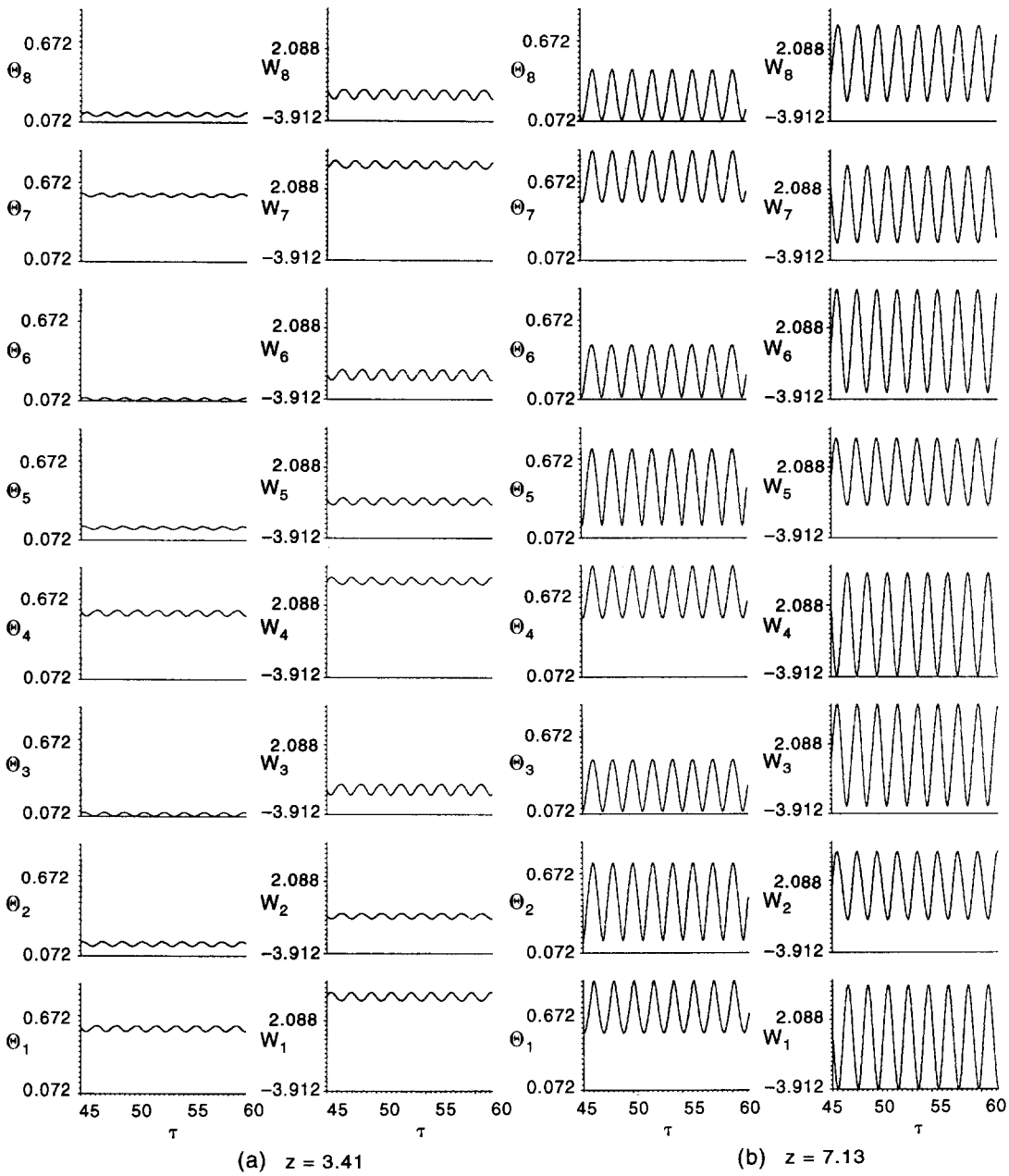

Fig. 6. Time samples at selected detection points for w and θ for $Re = 5$ and $Ra = 4300$ at cross-sections y(a) $z = 3.41$ and (b) $z = 7.13$.

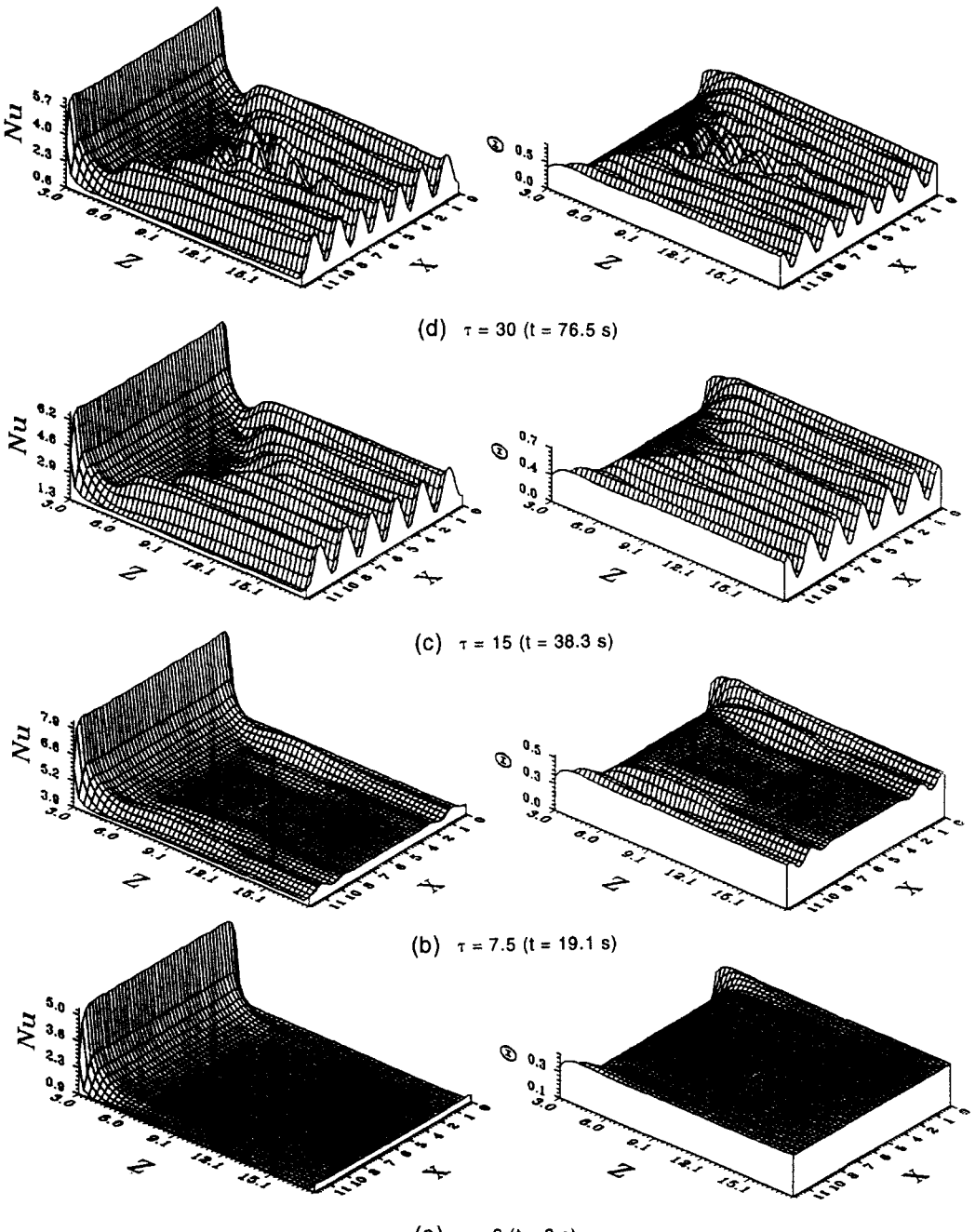

Fig. 7. The local Nusselt number distribution on the bottom plate and the temperature distribution in the middle horizontal plane ($y = 0.5$) for $Re = 10$ and $Ra = 4200$ at eight selected time instants (a) $\tau = 0$ ($t = 0$); (b) $\tau = 7.5$ ($t = 19.1$ s); (c) $\tau = 15$ ($t = 38.3$ s); (d) $\tau = 30$ ($t = 76.5$ s); (e) $\tau = 37.5$ ($t = 95.6$ s); (f) $\tau = 45$ ($t = 114.8$ s); (g) $\tau = 55$ ($t = 140.3$ s); (h) $\tau = 65$ ($t = 165.8$ s). (*Continued overleaf.*)

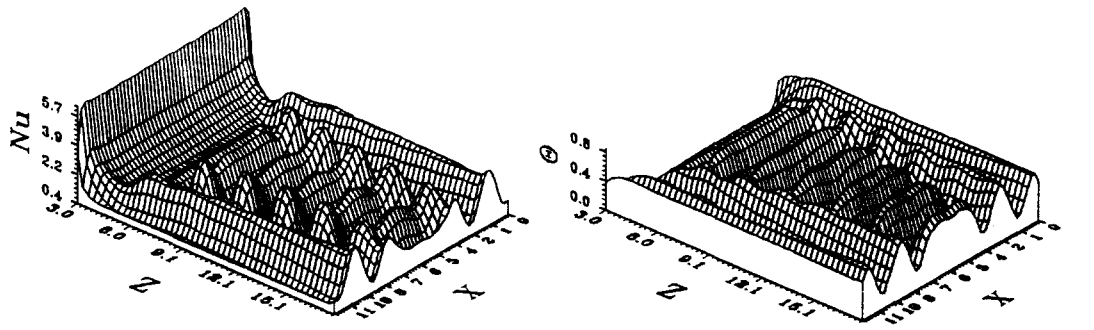

(h) $\tau = 65$ (t = 165.8 s)

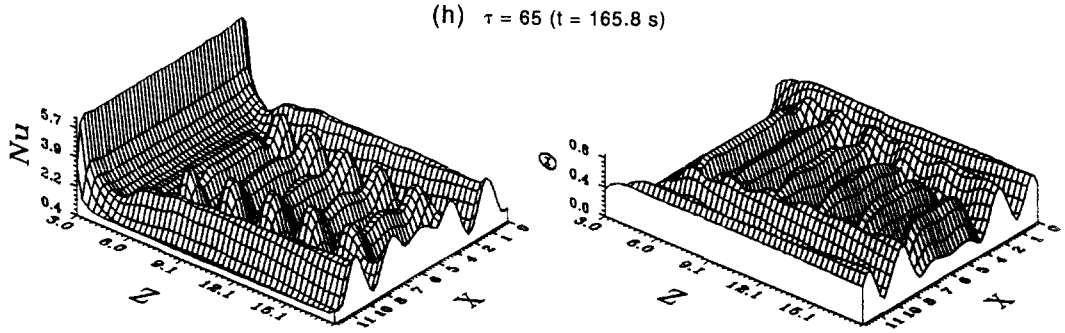

(g) $\tau = 55$ (t = 140.3 s)

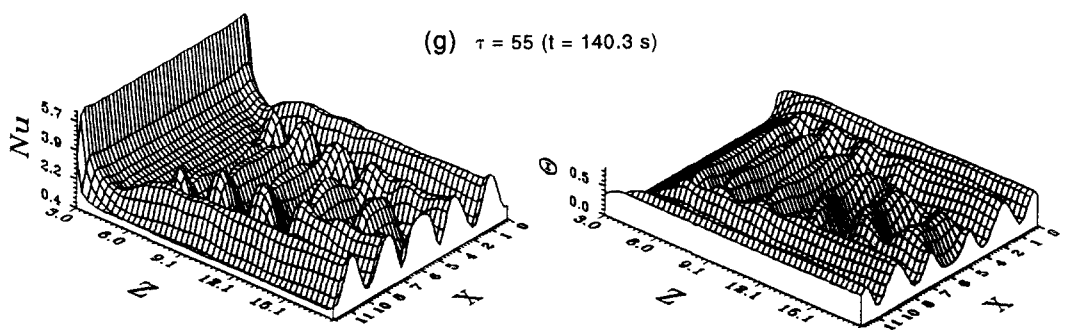

(f) $\tau = 45$ (t = 114.8 s)

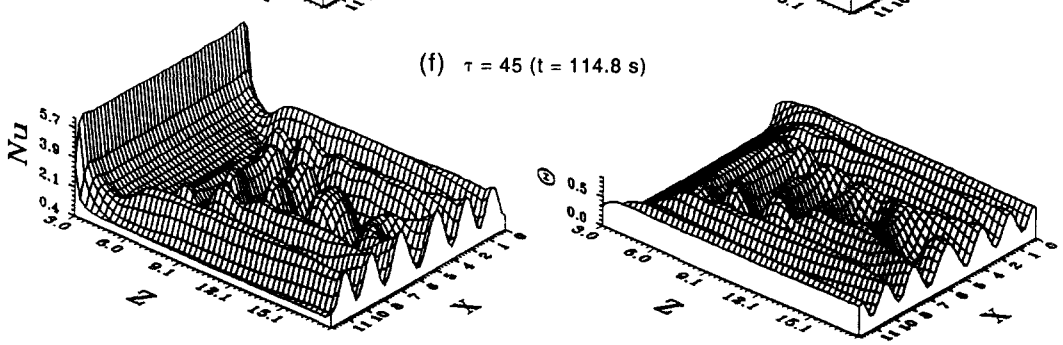

(e) $\tau = 37.5$ (t = 95.6 s)

Fig. 7—*continued.*

detailed formation of transverse and mixed longitudinal and transverse vortex rolls, from the subcritical flow, in the mixed convection of air in a bottom heated horizontal flat duct. In the early transient the flow is always dominated by the longitudinal rolls near the duct sides. The later induced transverse rolls in the duct entry get stronger with time and move downstream to push the longitudinal rolls in front of them out of the duct. At low Reynolds numbers the transverse rolls are longer and stronger to expel the longitudinal rolls in the side wall region out of the duct. Thus, a pure and regular transverse roll pattern results. But at a higher Reynolds number the transverse rolls are shorter and weaker and the longitudinal rolls stay near the duct sides to form a mixed roll structure. The experimentally observed and numerically predicted vortex pattern are in qualitative agreement.

It should be pointed out that the detailed transformation processes from one vortex flow pattern to

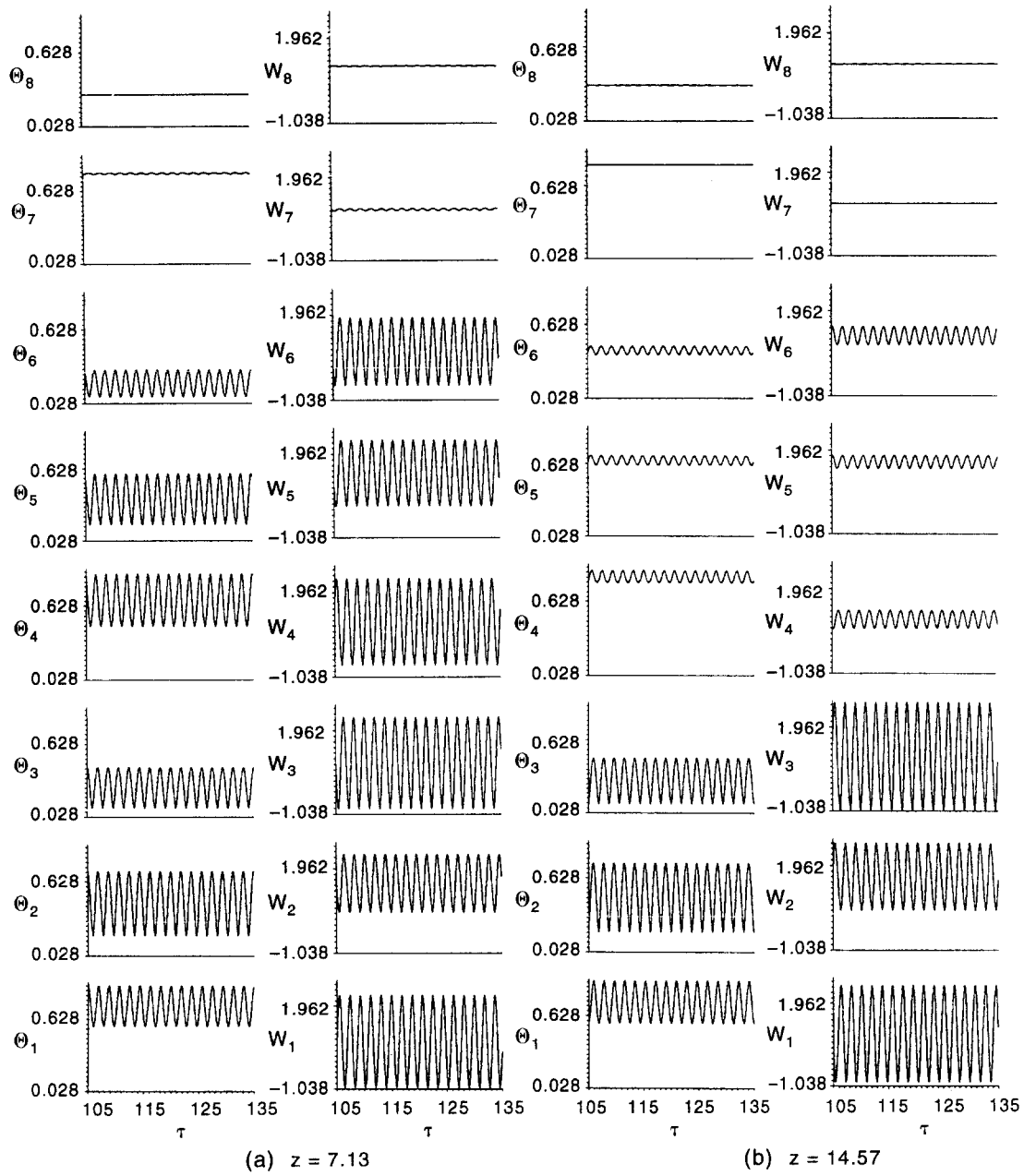

Fig. 8. Time samples at selected detection points for w and θ for $Re = 10$ and $Ra = 4200$ at cross-sections (a) $z = 7.13$ and (b) $z = 14.57$.

another, such as the change from the longitudinal to the transverse rolls or to mixed rolls or the reverse processes, are also relatively important in many technological applications and need to be explored in the future.

Acknowledgement—The financial support of this study by the engineering division of National Science Council of Taiwan, Republic of China through contract NSC83-0404-E009-054 is greatly appreciated.

REFERENCES

1. Evan, G. and Grief, R., A study of traveling wave instabilities in a horizontal channel flow with application to chemical vapor deposition. *International Journal of Heat and Mass Transfer*, 1989, **32**, 985–911.
2. Hwang, C. C. and Lin, T. F., Buoyancy induced flow transition in mixed convective flow of air through a bottom heated horizontal rectangular duct. *International Journal of Heat and Mass Transfer*, 1994, **37**, 1235–1255.
3. Mori, Y. and Uchida, Y., Forced convective heat transfer between horizontal flat plates. *International Journal of Heat and Mass Transfer*, 1996, **9**, 803–817.
4. Akiyama, M., Hwang, G. J. and Cheng, K. C., Experiments on the onset of longitudinal vortices in laminar forced convection between horizontal planes. *Journal of Heat Transfer*, 1971, **93**, 335–341.
5. Hwang, G. J. and Liu, C. L., An experimental study of convective instability in the thermal entrance region of a horizontal parallel-plate channel heated from below.

Canadian Journal of Chemical Engineering, 1976, **54,** 521–525.
6. Lee, F. S. and Hwang, G. J., Transient analysis on the onset of thermal instability in the thermal entrance region of a horizontal parallel plate channel. *Journal of Heat Transfer*, 1991, **113,** 363–370.
7. Ostrach, S. and Kamotani, Y., Heat transfer augmentation in laminar fully developed flow by means of heating from below. *Journal of Heat Transfer*, 1975, **97,** 220–225.
8. Kamotani, Y. and Ostrach, S., Effect of thermal instability on thermally developing channel flow. *Journal of Heat Transfer*, 1976, **98,** 62–66.
9. Chiu, K. C. and Rosenberger, F., Mixed convection between horizontal plates—I. Entrance effects. *International Journal of Heat and Mass Transfer*, 1987, **30,** 1645–1654.
10. Chiu, K. C. and Rosenberger, F., Mixed convection between horizontal plates—II. Fully developed flow. *International Journal of Heat and Mass Transfer*, 1987, **30,** 1655–1662.
11. Luijkx, J. M. and Platten, J. K., On the existence of thermoconvective rolls transverse to a superimposed mean poiseuille flow. *International Journal of Heat and Mass Transfer*, 1981, **24,** 1287–1291.
12. Ouazzani, M. T., Caltagirone, J. P., Meyer, G. and Mojtabi, A., Etude numérique et expérimental de la convection mixte entre deux plans horizontaux. *International Journal of Heat and Mass Transfer*, 1989, **32,** 261–269.
13. Ouazzani, M. T., Platten, J. K. and Mojtabi, A., Etude expérimental de la convection mixte entre deux plans horizontaux à températures defferents—II. *International Journal of Heat and Mass Transfer*, 1990, **33,** 1417–1427.
14. Yu, C. H., Chang, M. Y. and Lin, T. F., Structures of moving transverse and mixed rolls in mixed convection of air in a horizontal plane channel. *International Journal of Heat and Mass Transfer*, 1997, **40,** 333–346.
15. Kline, S. J. and McClintock, F. A., Describing uncertainties in single-sample experiments. *Mechanical Engineering*, 1953, **75,** 3–12.
16. Abernethy, R. B. and Thompson, Jr, J. W., Handbook—uncertainty in gas turbine measurement. Technical report No. AEDC-TR-73-5 (AD-755256), 1973.
17. Shah, R. K. and London, A. L., *Laminar Flow Forced Convection in Ducts*. Academic Press, New York, 1978, pp. 196–198.
18. Peyret, R. and Taylor, T. D. *Computational Methods for Fluid Flow*, Chap. 6. Springer–Verlag, New York, 1983.
19. Hirsch, C., *Numerical Computation of Internal and External Flow*, Vol. I. Wiley, New York, 1989, pp.176–179.
20. Kawamura, T., Takami, H. and Kuwahara, K., New higher-order upwind scheme for incompressible navier–stokes equations. *Ninth ICNMFD*, Vol. 10 (1985), pp. 285–291.
21. Anderson, D. A., Tannehill, J. C. and Pletcher, R. H., *Computational Fluid Mechanics and Heat Transfer*. Hemisphere, Washington, DC, 1984, pp. 71–77.